

Scale matters: simulation of nanoscopic dendrite initiation in the lithium solid electrolyte interphase using a machine learning potential

Sherif Abdulkader Tawfik,^{1,*} Linh La,¹ Tri Minh Nguyen,¹ Truyen Tran,¹ Sunil Gupta,¹ and Svetha Venkatesh¹

¹Applied Artificial Intelligence Institute, Deakin University, Geelong, Victoria 3216, Australia.

Although lithium solid state electrolytes promise to mitigate the chemical instabilities of liquid electrolytes in today's mainstream rechargeable batteries, solid state electrolytes still suffer from dendrite formation which leads to battery degradation and short circuiting. Dendrite initiation and propagation in specific solid state electrolyte materials has been explained, at a microscopic scale, as emerging from the lithium-filling of pores within the solid state electrolytes via microcracks. At the atomistic scale, the thermodynamic instability of many solid state electrolyte materials can explain their susceptibility to crystal decomposition upon contact with the lithium anode. However, for a more complete picture of the dendrite formation mechanisms, an understanding of the dendrite initiation mechanism at the intermediate nanoscopic scale is required. This work applies a machine learning potential (DIEP) for simulating six different solid state electrolyte-lithium interfaces at 300 K and 1000 K, with model sizes ranging from 18k to 36k atoms, for durations exceeding 20 ps. Our simulations show that the lithium dendrite initiation process can have an underpinning nanoscopic mechanism, in which the crystal decomposition by direct lithium interaction leads to the clustering of lithium. The simulations also suggest a possible mechanism for the creation of voids within the solid-electrolyte interphase, which have been observed in the Li|Li₆PS₅Cl|Li interface.

I Introduction

To satisfy the ever-growing need for durable and safe battery materials, lithium solid state electrolytes (SSEs) are believed to revolutionise the battery industry by substituting the liquid electrolyte in today's batteries (which are flammable and unstable under temperature extremes) with a solid inflammable material.¹ However, interfacial instability and resistance are among the most difficult challenges facing SSEs:² This includes synthesis conditions and sample purity that contribute to the formation of the Li-resistant solid-electrolyte interphase layer and the growth of lithium dendrites. The most critical challenge against the broad adoption of SSEs is interfacial instability at the lithium metal interface. The thermodynamics of a number of SSE materials at the lithium metal interface were examined by Zhu et al.³

Several works, such as the seminal work by Mo et al.,⁴

have established the utility of *ab initio* molecular dynamics (AIMD) in simulating the diffusion of lithium in solid structures. The key to the capability of AIMD in such simulations is that it applies density functional theory (DFT) for the computation of the atomic forces, rather than using empirical force fields in classical molecular dynamics approaches that have traditionally been the workhorse simulators of lithium diffusion in liquid and polymer electrolytes.⁵

However, the accuracy advantage brought by AIMD is accompanied by a scalability disadvantage: there is a harsh limit to the system size that can be simulated, given that DFT computations scale as N^3 where N is the system size (such as the number of atoms), making it infeasible to model simulation cells with more than 500 atoms for a few hundred picoseconds. This is unlike the situation in classical molecular dynamics in which hundreds of thousands of atoms can be feasibly simulated for time periods exceeding nanoseconds. Although large SSE models might not be required for an accurate estimation of the lithium ionic conductivity, studying interface phenomena typically involves large struc-

* s.abbas@deakin.edu.au

55 tures that exceed several thousand atoms because such phe-
 56 nomena occur at length scales that exceed a few nanometers
 57 (the length scale that is feasible for AIMD simulations). For
 58 example, only small atomic phenomena were observed in the
 59 228-large simulation cell for the lithium metal|Li₆PS₅Cl in-
 60 terface after 500 ps.⁶ Importantly, modeling a SSE requires a
 61 framework that can accurately represent the binding between
 62 the mobile cation, which in the present case is the lithium
 63 cation Li⁺, and the atoms in the structure. Classical molec-
 64 ular has traditionally been the method of choice for simula-
 65 ting the diffusion of lithium in liquid electrolyte solutions and
 66 polymers.

67 The quantum mechanical precision of DFT can, however,
 68 be “learnt” and transferred to large length scales and long
 69 time scales with the help of machine learning (ML) force
 70 fields. A number of ML force field models have recently
 71 been introduced,^{7,8} and the M3GNET force field by Chen
 72 and Ong⁸ has particularly attracted attention owing to its im-
 73 proved accuracy and transferrability to various material com-
 74 positions and sizes. The M3GNET is a physics-informed
 75 ML model that employs deep graph neural networks, and
 76 was trained on 188k samples to predict the total energy/atom,
 77 atomic forces and lattice stress. The direct integration of the
 78 external potential (DIEP) model, which improved the phys-
 79 ical insight on which DimeNet, M3GNET and other PIML
 80 models are based, was demonstrated to surpass the accuracy
 81 of M3GNET for a number of use cases.⁹

82 This work applies the DIEP force field to examine the
 83 interfacial phenomena in lithium metal|SSE interface for a
 84 selection of high conductivity SSE materials, including the
 85 well-known Li₁₀GeP₂S₁₂,¹⁰ Li₆PS₅Cl,¹¹ Li₇La₃Zr₂O₁₂,¹²
 86 and the ones predicted to have high conductivity in Ref.:¹³
 87 CsLi₂I₃, LiGaI₄ and LiGaBr₃. By modelling large simula-
 88 tion structures that have > 20k atoms, we were able to ob-
 89 serve the creation of the SEI decomposition products, the
 90 diffusion of anions into the lithium metal, the generation of
 91 a lithium void at the Li|Li₆PS₅Cl interface, and the high re-
 92 sistance of Li₇La₃Zr₂O₁₂ to decomposition.

TABLE 1. The material IDs and the formulas for the SSE structures examined in this work. The decomposition products are computed using the energies available in the MP database for the stable competing phases. The decomposition energy is defined in Equation 1.

MP ID	Formula	Decomposition products	Decomposition energy (meV)
mp-567967	LiGaI ₄		
mp-28327	LiGaBr ₃		
mp-942733	Li ₇ La ₃ Zr ₂ O ₁₂	Li ₆ Zr ₂ O ₇ + $\frac{3}{2}$ La ₂ O ₃ + $\frac{1}{2}$ Li ₂ O	-6
mp-569055	CsLi ₂ I ₃	CsI + 2LiI	-17
mp-696138	Li ₁₀ GeP ₂ S ₁₂	2Li ₃ PS ₄ + Li ₄ GeS ₄	-19
mp-985592	Li ₆ PS ₅ Cl	Li ₃ PS ₄ + LiCl + Li ₂ S	-82

93 II Computational details

94 To build our model systems, we obtain the structures of the
 95 SSE materials from the Materials Project (MP) database.¹⁴
 96 The material IDs for the structures are provided in Table 1.
 97 Note that, for Li₁₀GeP₂S₁₂, we are using the same structure
 98 that was used in Ref..³ While the structures of LiGaI₄ and
 99 LiGaBr₃ in the MP database correspond to the ground state
 100 phases of the materials, and Li₇La₃Zr₂O₁₂ is an experimen-
 101 tal stable phase, the structures of Li₁₀GeP₂S₁₂ and Li₆PS₅Cl
 102 are metastable phases. We present the structural decomposi-
 103 tion products and decomposition energies (or energy above
 104 hull) for these structures in Table 1. For a given decompo-
 105 sition reaction, say $A \rightarrow B + C$, the decomposition energy
 106 ΔE is computed as

$$\Delta E = E_B + E_C - E_A \quad (1)$$

107 where E_B , E_C and E_A are the total energies for structures A ,
 108 B and C , respectively. This value corresponds to the energy
 109 above hull, which determines the thermodynamic stability of
 110 a crystal structure.

111 Each of the SSE structures in Table 1 is then used for the
 112 creation of a lithium metal|SSE interface structure. First,
 113 a cubic supercell is generated for the SSE structure using
 114 the CubicSupercellTransformation class in the
 115 pymatgen python library (for the SSE supercells that are
 116 non-cubic). Then, a commensurate SSE|lithium interface is
 117 build, in which the lithium interface surface is the (110) facet
 118 of bcc lithium (mp-51). In the initial structure, a space of

TABLE 2. The number of atoms in the simulation supercell and simulation durations at 300 K and 1000 K (in ps) for each of the 6 interface structures.

Interface	Number of atoms	Duration at 300 K (ps)	Duration at 1000 K (ps)
LiGaI ₄	24,960	50.21	48.95
LiGaBr ₃	28,280	30.45	31.83
Li ₇ La ₃ Zr ₂ O ₁₂	17,520	32.03	27.04
CsLi ₂ I ₃	24,480	45.87	46.16
Li ₁₀ GeP ₂ S ₁₂	23,600	38.45	38.03
Li ₆ PS ₅ Cl	35,520	24.61	22.99

2.5 Å is between the SSE and the lithium metal surface. While searching for commensurate supercells, we have allowed a lattice mismatch of up to 2% between the SSE and the lithium metal surface. The resulting number of atoms in each supercell is displayed in Table 2.

We have run our simulations using the DIEP potential model diep-pes which is distributed as part of the oganesson python package. The PES model was trained on the 188k-samples large MPF.2021.2.8 dataset.⁸ Details of the DIEP model are available in the main reference: Ref.⁹ The simulations were run at two temperatures: 300 K, to model the evolution of the SEI at ambient conditions, and 1000 K, to challenge the structural integrity of the SSE under high lithium current.

III Results and discussion

Bulk structures First, we compare the optimised lattice constants and volume that were computed using the DIEP potential model and the corresponding values available in the MP database. The results of the comparison are displayed in Table 3.

We examine the performance of the DIEP potential for predicting the diffusion properties of the bulk structures of the materials LiGaI₄, LiGaBr₃, Li₇La₃Zr₂O₁₂, CsLi₂I₃, Li₁₀GeP₂S₁₂ and Li₆PS₅Cl. We display the results in Figure S1. In the same figures, we display the corresponding

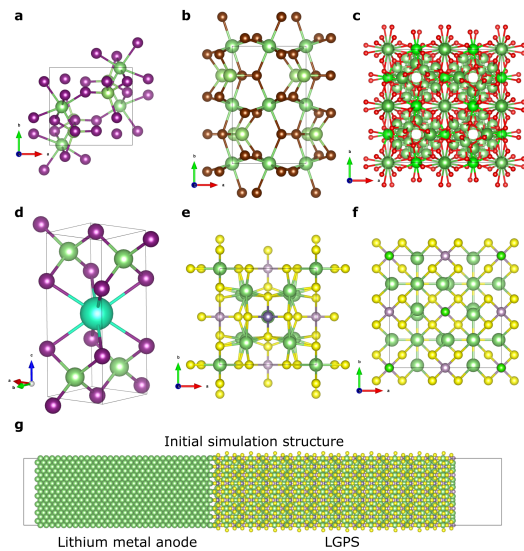


FIG. 1. (a-f) The unit cells of the solid state electrolyte materials: LiGaI₄, LiGaBr₃, Li₇La₃Zr₂O₁₂, CsLi₂I₃, Li₁₀GeP₂S₁₂ and Li₆PS₅Cl. (g) The structure of the simulation cell: the interface of the solid state electrolyte (right) and the lithium metal (left), and a 2.5 Å gap between them.

TABLE 3. The absolute error percentages for the predicted lattice parameters (a , b , c , α , β and γ) and the lattice volume V using the DIEP potential model, relative to the values in the MP database.

Lattice parameter	LiGaI ₄	LiGaBr ₃	Li ₇ La ₃ Zr ₂ O ₁₂	CsLi ₂ I ₃	Li ₁₀ GeP ₂ S ₁₂	Li ₆ PS ₅ Cl
a	1.3	6.2	0.4	4.0	0.8	1.5
b	3.7	5.1	0.4	4.0	0.8	1.5
c	5.2	2.1	0.1	2.0	0.2	1.5
α	0.0	0.0	0.0	0.0	0.0	0.0
β	1.7	4.0	0.0	0.0	0.0	0.0
γ	0.1	0.0	0.0	0.0	0.0	0.0
V	10.3	9.4	0.9	5.9	1.8	4.4

AIMD-calculated values for the diffusion coefficients: for LiGaI₄, LiGaBr₃, and Li₁₀GeP₂S₁₂, the AIMD values were obtained from Ref.;¹³ for Li₆PS₅Cl, the values were computed by us. We display the AIMD values as orange triangles in Figure S1 for comparison. DIEP over-estimates the values of the diffusion coefficients for low and high temperatures for Li₁₀GeP₂S₁₂ and CsLi₂I₃ with respect to the

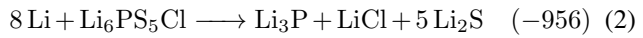
151 AIMD-predicted values, whereas it over-estimates the low
 152 temperature values for LiGaI₄ and LiGaBr₃. Given that the
 153 key properties we will focus on in this work are qualitative
 154 (lithium and metal clustering in the SEI), it is sufficient that
 155 the DIEP accurately reproduces the structural parameters.
 156 Over-estimating diffusivity is not expected to significantly
 157 impact these qualitative features, but will rather speed up
 158 their creation.

159 **SSE|Li models** For each of the six lithium metal anode|SSE
 160 structures in Table 2, the simulation at 300 K and 1000 K
 161 result in the diffusion of lithium from the anode into the
 162 SSE, accompanied with the breakdown of the lattice struc-
 163 ture of the SSE material close to the interface. We display
 164 the structure of the supercell at the end of each respective
 165 simulation time in Figure 2. For each interface, we display
 166 the initial, final interface structures side-by-side to highlight
 167 the difference in diffusivity trends between the different in-
 168 terfaces (displayed as the left, middle and right figures, re-
 169 spectively). We also show the final structure of the lithium
 170 anode alone to clarify the actual extent of the diffusion of
 171 lithium within the SSE structure.

172 The extent of lithium diffusion clearly corresponds to the
 173 computed diffusivity of the bulk supercell of the SSE in Fig-
 174 ure S1. The two SSEs with the highest diffusivity, LiGaI₄,
 175 LiGaBr₃, allow lithium atoms to diffuse very deeply into the
 176 SSE structure, as shown in Figures 2a and b. Due to the lim-
 177 ited size of the interface supercell compared with the actual
 178 physical structures, the lithium diffusion in LiGaBr₃ resulted
 179 in the drift of a large amount of Li atoms into the SSE struc-
 180 ture, resulting in the appearance of a gap at the bottom of
 181 the anode. The lithium atoms were detached from the frozen
 182 lithium atoms at the bottom of the structure. Diffusion into
 183 Li₇La₃Zr₂O₁₂ is the slowest, which agrees with the sluggish
 184 diffusion of this SSE reported in Ref.¹⁵ (Figure 2c). We mea-
 185 sure the diffusion of lithium from the anode into the SSE by
 186 calculating the Li⁺ current density, which we define as the
 187 number of Li⁺ crossing from the anode region into the SSE.
 188 The Li⁺ current density at 300 K is displayed in Figure 3.
 189 The results generally reflect those in Figure S1: diffusion

190 in Li₇La₃Zr₂O₁₂ results in the lowest Li⁺ current density,
 191 whereas LiGaI₄, LiGaBr₃ have the highest the lowest Li⁺
 192 current densities.

193 **Lithium clustering and dendrite formation** Lithium den-
 194 drites are known to form along the grain boundaries and
 195 pore (void) networks of SSEs.^{2,16–18} By examining the
 196 Li₆PS₅Cl|Li interface, Ning et al.² have distinguished be-
 197 tween two fundamental dendrite processes: dendrite *forma-*
 198 *tion* and dendrite *propagation*: dendrite formation is caused
 199 by the deposition of Li in pre-existing subsurface pores.^{18,19}
 200 A subsurface pore is a microscopic void that exists within
 201 the structure of the SSE, and can be connected to other pores
 202 or to the anode surface via microcracks. The dendrite initia-
 203 tion progresses by filling the pore, which happens due to the
 204 flow of lithium via the microcrack. Subsequent to filling of
 205 these pores, cracks form due to the increasing pressure ap-
 206 plied by the pores on the SSE, and then the crack propagates
 207 into the SSE towards the cathode. Crack propagation occurs
 208 before dendrite propagation; once the dendrite starts flowing
 209 through the crack, it reaches the cathode leading to short-
 210 circuiting. Hence, according to microscopic observations
 211 and models, voids within the SSE microstructure are the pri-
 212 mary culprit of dendrite formation. Atomistic modelling of
 213 the lithium deposition process suggest the chemical insta-
 214 bility of the Li₆PS₅Cl when in contact with the anode: the
 215 structure of the SSE is likely to rapidly decompose accord-
 216 ing to the equation.¹⁵ We display ΔE in units of meV/atom
 217 between brackets.



218 This equation is the same as the equation in Ref.⁶ for this
 219 SSE. Such structural instability might suggest nanoscopic
 220 dendrite initiation mechanisms upon lithium plating, even in
 221 the absence of grain boundaries. The results of the AIMD
 222 simulations within the NVT ensemble (constant temperature,
 223 constant volume) by Cheng et al.⁶ for Li₆PS₅Cl|Li show the
 224 penetration of small clusters of Li atoms into the SSE after
 225 500 ps. Their simulation model was 228 atoms, too small to

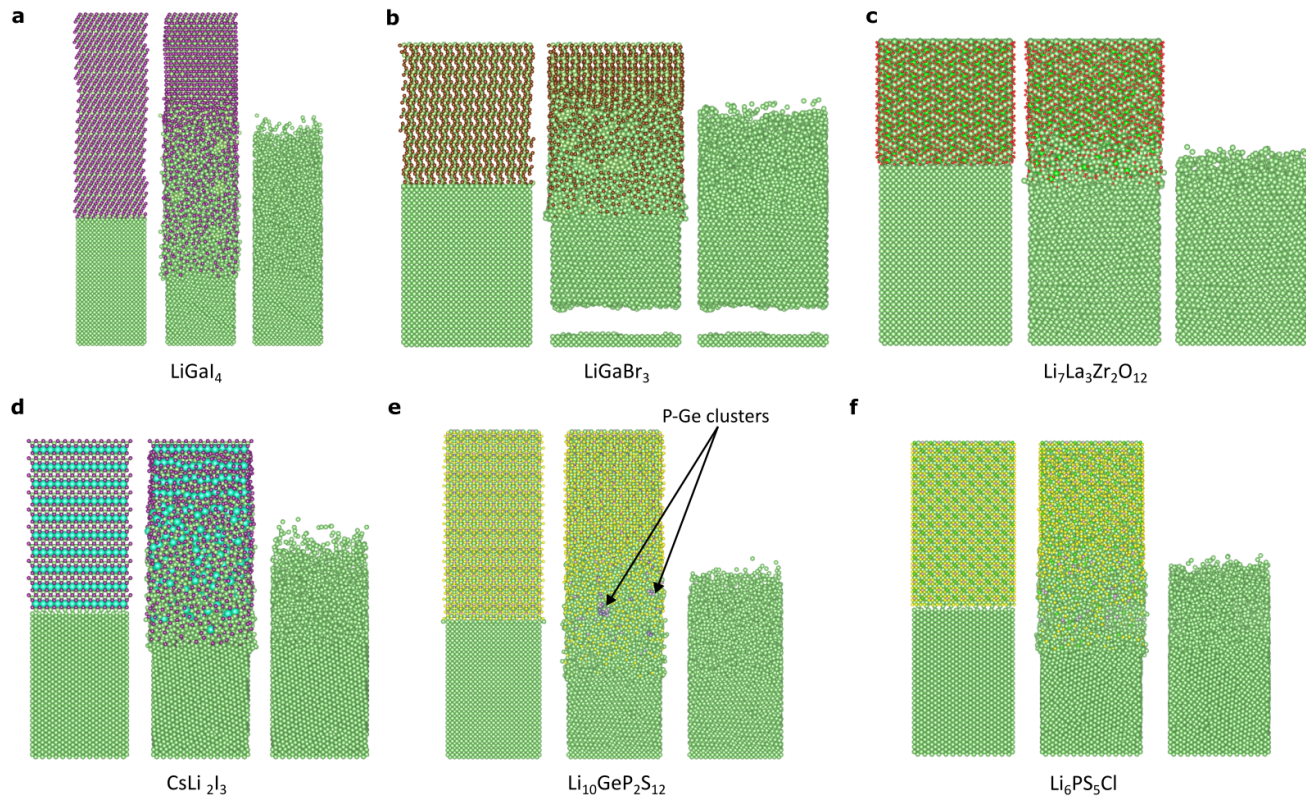


FIG. 2. The structure of the lithium metal | SSE interface after the MD simulations: (a) LiGaI₄, (b) LiGaBr₃, (c) Li₇La₃Zr₂O₁₂, (d) CsLi₂I₃, (e) Li₁₀GeP₂S₁₂ and (f) Li₆PS₅Cl. Each subfigure displays the entire interface before the simulation, the structure of the lithium anode after the simulation, and the structure of the interface after the simulation.

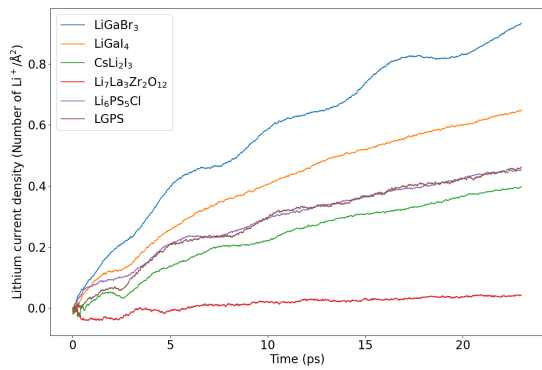


FIG. 3. Lithium current flow from the anode into the SSE.

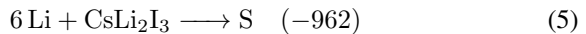
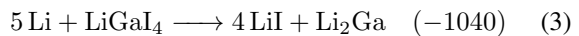
reveal any significant clustering phenomena. An interesting feature in these results is in Figure 4(c): the formation of a void within the SSE structure after 500 ps. We discuss SSE void formation in a later section.

Our simulations scale up the work in Ref.⁶ to examine the possible initiation of lithium dendrites at a nanoscopic scale. By examining the solid SSE structures without grain boundaries, we observe the creation of lithium clusters at the anode surface, which might initiate dendrite initiation. We highlight the lithium clusters at the interfaces in Figure S2. We examine the nucleation of lithium clusters by examining the accumulation of at least 6 Li atoms within spheres of radius 3 Å. This is based on the Li—Li bond length in the bcc bulk Li structure (3.06 Å) where each Li atom is directly bonded to 8 surrounding Li atoms. The existence of such lithium clusters within the SSE is an indication for the nucleation of lithium clusters, which are precursors for the formation of lithium dendrites. Lack of such lithium clusters implies that the Li atoms are diffusing evenly within the SSE.

229

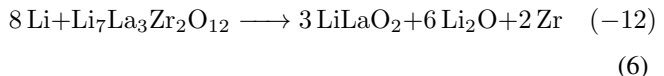
230
231
232
233
234
235
236
237
238
239
240
241
242
243
244

In LiGaI₄|Li, LiGaBr₃|Li and CsLi₂I₃|Li, rapid disintegration of the lattice structures would be expected, given their crystal instability in the presence of lithium atoms (Ref.¹⁵) the following reaction energies are highly exothermic.



However, the LiGaI₄|Li and CsLi₂I₃|Li in Figures S2(a,d) do not exhibit Li clusters in the SSE. LiGaBr₃|Li in Figure S2(b) exhibits three Li clusters inside the SSE which are separate from the Li anode. This means that lithium dendrites might not be likely to form LiGaI₄|Li and CsLi₂I₃|Li where, instead, Li⁺ ions are more likely to diffuse uniformly through the SSE structure.

The most Li-sluggish SSE material is Li₇La₃Zr₂O₁₂, which have the highest crystal stability against the Li interface (the decomposition energy is -12 meV/atoms, Equation 6 is from Ref.¹⁵):



However, the Li₇La₃Zr₂O₁₂|Li interface displays the protrusion of two Li clusters from the surface of the Li anode (indicated by circles in Figure S2(c)). This is despite the extremely low lithium current computed across this interface (Figure 3). However, it is unlikely that these protrusions will lead to further penetration of lithium structures into the lattice of Li₇La₃Zr₂O₁₂ because, as will be shown later, the lattice structure of Li₇La₃Zr₂O₁₂ is highly stabilised by its La—Zr framework.

The above analysis suggests that dendrite initiation in Li₇La₃Zr₂O₁₂|Li, LiGaI₄|Li and CsLi₂I₃|Li is not nanoscopic in nature, but instead, *is primarily the microscopic processes* in Ref..² The LiGaI₄ and CsLi₂I₃ SSE that was suggested by the screening in Ref.,¹³ hence, bring a significant advantage compared to the more well-known SSE

materials, Li₁₀GeP₂S₁₂ and Li₆PS₅Cl, as will be examined below.

Lithium clustering is far more prevalent in the Li₁₀GeP₂S₁₂|Li and the Li₆PS₅Cl|Li interfaces, as shown in Figures S2(e,f). Numerous Li clusters form in the SEI of these interfaces, which corroborates the highly exothermic crystal decomposition energies in these systems (Equations 7 is from Ref.¹⁵):



The significant lithium clustering at these two interfaces suggests that the lithium dendrite initiation process in these interfaces is the nanoscopic interfacial decomposition, in addition to the microscopic initiation process in Ref..² Such nanoscopic clustering processes would fracture the SSE structure close to the anode during the fabrication of the interface.

If simulations were conducted for longer time scales, we believe that the lithium clusters in Figure S2 will evolve into larger structures, or dendrites. It is worth noting that these simulations do not involve electrons, even though the evolution of lithium dendrites is an electron-dependent phenomenon. However, the ML model we have used, DIEP, is trained to reproduce the effect of electrons on the atomic structure of materials without learning directly the electron density of the structures. The training set of these ML models include the atomic positions and forces. By accurately predicting these quantities, the DIEP model can reliably predict the atomic positions and forces in various contexts, such as the context of dendrite formation at the lithium electrolyte interfaces.

Formation of metal phases A common decomposition product that is observed in the SEI of solid-state batteries is metal clusters, which is formed from the clustering of the metal elements (apart from pure lithium clusters) in the SSE material. The formation of these clusters is also implied by the thermodynamic consideration of Equations 2, 3, 4, 5, 6 and 7. We display the formation of the metal clusters in Fig-

ure S3 at the two simulation temperatures 300 K and 1000 K.

We account for a Ga cluster when a Ga atom is surrounded by at least 5 Ga atoms within a radius of 3 Å, given that the Ga—Ga bond distances in the ground state Ga structure (mp-142) range from 2.49 Å to 2.75 Å and each Ga atom is surrounded by 5 up to 7 Ga atoms. Based on this cluster assignment, we observe a few Ga clusters in the SEIs of both LiGaI₄|Li and LiGaBr₃|Li at 300 K, as shown in Figures S3(a,b). Example Ga clusters are displayed in Figures 4(a,b), where a bond is drawn for all Ga—Ga bonds that are smaller than 3 Å. The clusters disintegrate at 1000 K (Figure S3(a,b)) in both interfaces resulting in fewer and smaller clusters that are mainly distributed at the SSE side of the SEI.

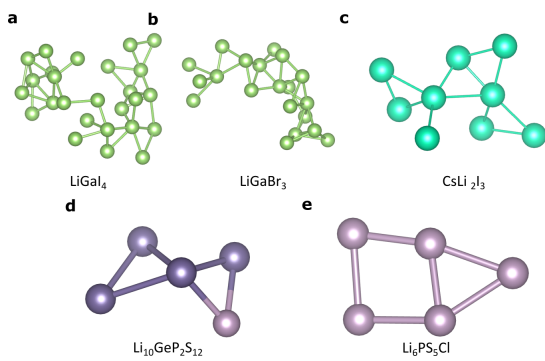


FIG. 4. The atomic structures of sample metal clusters from Figure S3.

The low conductivity of the Li₇La₃Zr₂O₁₂ SSE can be understood in light of the strong La—Zr framework of the structure in Figure 3(c). We account for La—Zr clusters by collecting all La and Zr atoms where each La or Zr is surrounded by 7 La or Zr atoms within a radius of 4 Å. This is based on the following: the La-Zr bond is 3.6 Å and each Zr surrounded by 12 La atoms (mp-131); each La is surrounded by 12 La atoms in the Zr unit cell mp-26; each Zr is surrounded by 12 Zr atoms in the Zr unit cell mp-131; no clusters form with $N > 7$. The La—Zr framework remains intact even at 1000 K, as shown in Figure S3(c). The CsLi₂I₃|Li interface shows a behaviour that is intermediate between solid framework in Li₇La₃Zr₂O₁₂|Li and flexible

Ga frameworks in the LiGaI₄|Li, LiGaBr₃|Li interfaces. We account for Cs clusters by counting Cs atoms that are surrounded by at least 5 Cs atoms within a sphere of radius 6 Å. This cluster assignment is based on the ground state Cs unit cell (mp-1055940) where each Cs is surrounded by 12 Cs atoms within a 6 Å radius (no Cs clusters formed with $N > 5$). However, owing to the relatively large Cs—Cs bond distance, the Cs framework experienced significant perturbation at both temperatures.

The Li₁₀GeP₂S₁₂ and Li₆PS₅Cl display the lowest amount of metal cluster formation, as shown in Figures S3(e,f). This is primarily due to the much lower concentrations of P/Ge elemental compositions in these SSEs. The formation of these clusters goes in parallel with the lithium dendrite initiation process discussed above, leading to the creation of an electrically conductive SEI that leads to cell degradation.²⁰ We assign P clusters in Li₆PS₅Cl by counting P atoms which have more than 3 P atoms surrounding them within a radius of 3 Å. In Li₁₀GeP₂S₁₂, we assign P—Ge clusters by counting Ge/P atoms where each atom is surrounded by at least 4 Ge/P atoms within a radius of 3 Å.

Voids in Li₆PS₅Cl The low density region observed in Ref.⁶ suggest a possible process for the formation of voids within the SEI of the Li₆PS₅Cl|Li interface. Our simulation exhibit a large void close to the anode surface, which we display in Figure 5(a). Void formation was reported in the Li₆PS₅Cl|Li interface by Kasemchainan *et al.*,²¹ as a consequence of the flow of lithium away from the interface region above a critical current density. To ascertain that the void formation in our simulations of the Li₆PS₅Cl|Li interface is not a computational artefact, we simulated another interface structure with the same number of atoms but different lattice structure. According to Figure 5(b), we find that the void formation persists in the other structure. We rule out the possibility that the void is cause by an over-estimation of the density of the SSE bulk structure by the DIEP potential model, given that the DIEP-predicted error in volume is only 4.4%, as shown in Table 3.

The emergence of these voids in the Li₆PS₅Cl|Li interface

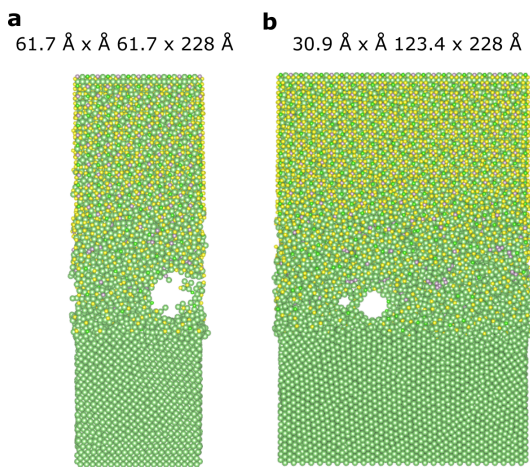


FIG. 5. Void formation in the $\text{Li}_6\text{PS}_5\text{Cl}|\text{Li}$ interface at 300 K in two simulation cells: (a) the original cell in Figure 1(f), and (b) a cell with different dimensions.

close to the anode surface indicates the spontaneous formation of voids upon the fabrication of the interface. The conclusion in Ref.²¹ states that charge-discharging the cell below a critical current might mitigate void formation, and hence dendrite formation. Our simulations reveal that void formation at this particular interface is inevitable, and can be avoided by applying external pressure, as the authors of Ref.²¹ have concluded, or possibly by chemical modification or microstructuring of the SSE.

It is worth noting that the fabrication process of the SSE-anode interface leaves numerous interfacial voids, which are known to have negative side effects such as the increase in the interface resistance.²⁰ Such voids between the SSE and the anode will require much larger interface models, and will be examined in future work.

IV Conclusion

To sum up, we were able to obtain qualitative knowledge on the structure of the solid-electrolyte interphase, formed by a solid state electrolyte and the lithium anode by performing

ab initio molecular dynamics simulations using a machine learning potential model, DIEP, with simulation cells that have tens of thousands of atoms. The solid state electrolytes we examined are LiGaI_4 , LiGaBr_3 , $\text{Li}_7\text{La}_3\text{Zr}_2\text{O}_{12}$, CsLi_2I_3 , $\text{Li}_{10}\text{GeP}_2\text{S}_{12}$ and $\text{Li}_6\text{PS}_5\text{Cl}$, which were chosen owing to their popularity in the literature or due to their predicted exceptionally high lithium conductivity. We found that the lithium diffusion across the $\text{Li}_7\text{La}_3\text{Zr}_2\text{O}_{12}|\text{Li}$, $\text{LiGaI}_4|\text{Li}$ and $\text{CsLi}_2\text{I}_3|\text{Li}$ interfaces is not accompanied with the formation of lithium clusters, which means that the lithium dendrite initiation process in these interfaces can be the microscopic process explored in Ref.,² but not a nanoscopic process that takes place across a clean interface (that is, an interface with no existing cracks or grain boundaries). However, a nanoscopic dendrite initiation process takes place across the $\text{LiGaBr}_3|\text{Li}$, $\text{Li}_{10}\text{GeP}_2\text{S}_{12}|\text{Li}$ and $\text{Li}_6\text{PS}_5\text{Cl}|\text{Li}$ interfaces, as the formation of lithium clusters was observed in the simulations close to the anode surface. By monitoring the metal cluster formation (that is, the clustering of the cationic species apart from lithium), we found that metal clusters form in the SEI of all of the interfaces except for $\text{Li}_7\text{La}_3\text{Zr}_2\text{O}_{12}|\text{Li}$ and $\text{CsLi}_2\text{I}_3|\text{Li}$, where the metal frameworks were significantly more rigid than in the other SSEs. The La—Zr framework in $\text{Li}_7\text{La}_3\text{Zr}_2\text{O}_{12}$ was particularly resistant to perturbation, which explains the sluggish diffusion of lithium in this SSE. Of particular interest is the $\text{Li}_6\text{PS}_5\text{Cl}|\text{Li}$ interface, in which the simulations exhibited the emergence of a void (vacuum region). We found that such void formation might echo a density functional theory-based *ab initio* molecular dynamics simulation, and importantly explains a recent experimental observation of such voids in the same interface.

References

- [1] A. Manthiram, X. Yu, and S. Wang, Lithium battery chemistries enabled by solid-state electrolytes, *Nat Rev Mater* **2**, 16103 (2017).
- [2] Z. Ning, G. Li, D. L. R. Melvin, Y. Chen, J. Bu, D. Spencer-Jolly, J. Liu, B. Hu, X. Gao, J. Perera, C. Gong, S. D. Pu, S. Zhang, B. Liu, G. O. Hartley, A. J. Bodey, R. I. Todd, P. S. Grant, D. E. J. Armstrong, T. J. Marrow, C. W. Monroe, and P. G. Bruce, Dendrite initiation and propagation in lithium metal solid-state batteries, *Nature* **618**, 287 (2023).
- [3] Y. Zhu, X. He, and Y. Mo, Origin of Outstanding Stability in the Lithium Solid Electrolyte Materials: Insights from Thermodynamic Analyses Based on First-Principles Calculations, *ACS Appl. Mater. Interfaces* **7**, 23685 (2015).
- [4] Y. Mo, S. P. Ong, and G. Ceder, First Principles Study of the Li₁₀GeP₂S₁₂ Lithium Super Ionic Conductor Material, *Chem. Mater.* **24**, 15 (2012).
- [5] H. G. Lee, S. Y. Kim, and J. S. Lee, Dynamic observation of dendrite growth on lithium metal anode during battery charging/discharging cycles, *npj Comput Mater* **8**, 103 (2022).
- [6] T. Cheng, B. V. Merinov, S. Morozov, and W. A. Goddard, Quantum Mechanics Reactive Dynamics Study of Solid Li-Electrode/Li₆PS₅Cl-Electrolyte Interface, *ACS Energy Lett.* **2**, 1454 (2017).
- [7] O. T. Unke, S. Chmiela, H. E. Sauceda, M. Gastegger, I. Poltavsky, K. T. Schütt, A. Tkatchenko, and K.-R. Müller, Machine Learning Force Fields, *Chem. Rev.* **121**, 10142 (2021).
- [8] C. Chen and S. P. Ong, A universal graph deep learning interatomic potential for the periodic table, *Nat Comput Sci* **2**, 718 (2022).
- [9] S. A. Tawfik, T. M. Nguyen, S. P. Russo, T. Tran, S. Gupta, and S. Venkatesh, Embedding material graphs using the electron-ion potential: application to material fracture (2024), arXiv:2402.10931 [cond-mat.mtrl-sci].
- [10] N. Kamaya, K. Homma, Y. Yamakawa, M. Hirayama, R. Kanno, M. Yonemura, T. Kamiyama, Y. Kato, S. Hama, K. Kawamoto, and A. Mitsui, A lithium superionic conductor, *Nature Mater* **10**, 682 (2011).
- [11] H. Deiseroth, S. Kong, H. Eckert, J. Vannahme, C. Reiner, T. Zaiß, and M. Schlosser, Li₆PS₅X: A Class of Crystalline Li-Rich Solids With an Unusually High Li⁺ Mobility, *Angew Chem Int Ed* **47**, 755 (2008).
- [12] R. Murugan, V. Thangadurai, and W. Weppner, Fast Lithium Ion Conduction in Garnet-Type Li₇La₃Zr₂O₁₂, *Angew Chem Int Ed* **46**, 7778 (2007).
- [13] L. Kahle, A. Marcolongo, and N. Marzari, High-throughput computational screening for solid-state Li-ion conductors, *Energy & Environmental Science* **13**, 928 (2020).
- [14] A. Jain, S. P. Ong, G. Hautier, W. Chen, W. D. Richards, S. Dacek, S. Cholia, D. Gunter, D. Skinner, G. Ceder, and K. A. Persson, Commentary: The Materials Project: A materials genome approach to accelerating materials innovation, *APL Materials* **1**, 011002 (2013).
- [15] S. Tawfik, J. Berk, T. Walsh, S. Rana, and S. Venkatesh, Accelerated discovery of solid-state electrolytes using Bayesian optimisation (2024).
- [16] S. Lou, F. Zhang, C. Fu, M. Chen, Y. Ma, G. Yin, and J. Wang, Interface Issues and Challenges in All-Solid-State Batteries: Lithium, Sodium, and Beyond, *Advanced Materials* **33**, 2000721 (2021).
- [17] Z. Ning, D. S. Jolly, G. Li, R. De Meyere, S. D. Pu, Y. Chen, J. Kasemchainan, J. Ihli, C. Gong, B. Liu, D. L. R. Melvin, A. Bonnin, O. Magdysyuk, P. Adamson, G. O. Hartley, C. W. Monroe, T. J. Marrow, and P. G. Bruce, Visualizing plating-induced cracking in lithium-anode solid-electrolyte cells, *Nat. Mater.* **20**, 1121 (2021).
- [18] Y. Ren, Y. Shen, Y. Lin, and C.-W. Nan, Microstructure Manipulation for Enhancing the Resistance of Garnet-Type Solid Electrolytes to “Short Circuit” by Li Metal Anodes, *ACS Appl. Mater. Interfaces* **11**, 5928 (2019).
- [19] L. Barroso-Luque, Q. Tu, and G. Ceder, An Analysis of Solid-State Electrodeposition-Induced Metal Plastic Flow and Predictions of Stress States in Solid Ionic Conductor Defects, *J. Electrochem. Soc.* **167**, 020534 (2020).
- [20] J. Liu, H. Yuan, H. Liu, C. Zhao, Y. Lu, X. Cheng, J. Huang, and Q. Zhang, Unlocking the Failure Mechanism of Solid State Lithium Metal Batteries, *Advanced Energy Materials* **12**, 2100748 (2022).
- [21] J. Kasemchainan, S. Zekoll, D. Spencer Jolly, Z. Ning, G. O. Hartley, J. Marrow, and P. G. Bruce, Critical stripping current leads to dendrite formation on plating in lithium anode solid electrolyte cells, *Nat. Mater.* **18**, 1105 (2019).